research papers

CrossMark

Optimization of the design for beamline with fast polarization switching elliptically polarized undulators

Jiefeng Cao, Yong Wang,* Ying Zou, Xiangzhi Zhang, Yanqing Wu* and Renzhong Tai*

Shanghai Institute of Applied Physics, Chinese Academy of Sciences, Shanghai 201800, People's Republic of China. *Correspondence e-mail: wangyong@sinap.ac.cn, wuyanqing@sinap.ac.cn, tairenzhong@sinap.ac.cn

Fast switching of X-ray polarization with a lock-in amplifier is a good method for acquiring weak signals from background noise for X-ray magnetic circular dichroism (XMCD) experiments. The usual way to obtain a beam with fast polarization switching is to use two series of elliptically polarized undulators (tandem twin EPUs). The two EPUs generate two individual beams. Each beam has a different polarization and is fast switched into the beamline. It is very important to ensure that the energy resolution, the flux and the spot size at the sample of the two beams are equal in XMCD experiments. However, it is difficult in beamline design because the distances from the two EPUs to the beamline optics are different and the beamline is not switchable. In this work, a beamline design without an entrance slit for fast polarization switching EPUs is discussed. The energy resolution of the two beams can be tuned to be equal by minor rotation of the optics in the monochromator. The flux of the two beams can be balanced through separation blades X, Y in the exit slit, and by adjusting the position of the X blades along the beam. The spot size of the two beams can be adjusted to be equal by shifting the sample as well.

1. Introduction

X-ray magnetic circular dichroism (XMCD) is the difference between the absorptions of left and right circularly polarized X-rays. The XMCD method using the polarization characteristics of the X-rays produced by an undulator provides a unique insight in the research field of magnetic materials and anisotropic systems. On account of this feature, XMCD beamlines have been built in almost every synchrotron radiation facility around the world. In some experiments, such as measuring natural circular dichroism (CD) for biomolecules, the CD signals often have low intensities comparable with noise; one way to enhance the signal-to-noise ratio is by modulating the helicity of the circularly polarized beam and measuring with a lock-in amplifier (Muro et al., 2005).

In order to achieve a fast polarization switching of the X-rays, the insertion device should be specially devised in the design of the beamline. Until now, the fast-switching sources are roughly classified into four types. The first type uses a permanent magnet elliptically polarized undulator (EPU); the polarization of the emitted X-ray beam is changed by only mechanically shifting permanent magnet arrays (Agui et al., 2001). The highest switching frequency is only 0.1 Hz because the helicity modulation (HM) speed is limited by the mechanical ability. The second type uses an electromagnet/permanent magnet hybrid undulator (EMPHU), where the highest frequency, in theory, can reach 100 Hz (Chavanne et

al., 1998; Tanaka *et al.*, 2002). The third type uses two helical undulators, the left and the right helical polarized X-ray beams emit from the two undulators. The two beams converge at the sample position from different directions (Sawhney *et al.*, 1997; Weiss *et al.*, 2001; Schmidt *et al.*, 2001). In this case, a high HM frequency is easily achieved by a chopper but the operation of optical elements is complicated on account of the different beam paths. The fourth type also uses two helical undulators, but the right and the left circularly polarized photon beams are emitted on the same axis; the two beams are switched by five kicker magnets (Hara *et al.*, 1998; Saitoh *et al.*, 1998, 2000), so-called tandem twin EPUs.

In this study, the last type of switching is adopted. Compared with the second type (EMPHU), a permanent magnet undulator is easy to produce and is more reliable. Compared with the third type, because the right and left circularly polarized photon beams are emitted on the same axis, the distributions of two beams in horizontal phase space are approximately the same and the operation of optical elements can be simple (Hara *et al.*, 2003). However, the design of the tandem twin EPUs also brings other difficulties. The difference in the positions of the two EPUs brings differences in energy resolution, flux and the spot size at the sample.

An XMCD signal is the difference between the absorption of left and right circularly polarized beams for a magnetic material, so it is important to ensure that, except for the polarity, the two polarized beams at the sample have the same properties. The differences in photon energy, energy resolution, flux and spot size need to be brought to our attention and are worth careful discussion. In this article, we give a design for this kind of beamline, which makes the energy resolution, the flux and the spot size equal in an easy way. The energy difference, which is a consequence of the two electron orbits in the two EPUs not at the same height or which have a canted angle to each other, can be controlled in an acceptable range with current accelerator technology, which is outside the scope of this article.

2. Beamline description

The insertion device adopts a tandem twin EPU switching system, which has been mentioned above. As shown in Fig. 1, two undulators and five kicker magnets are installed in a tandem configuration: one kicker magnet is placed in the center, two kicker magnets are placed before the two undulators and two afterwards. The five fast switching chicane magnets effectively select which light from the undulator passes through the beamline aperture. The length of each undulator is 1.6 m and the period is 50 mm, and the distance between the two undulators is 1 m. The midpoint of the straight section is chosen as the coordinate origin.

There are two ways to design this beamline, one with an entrance slit
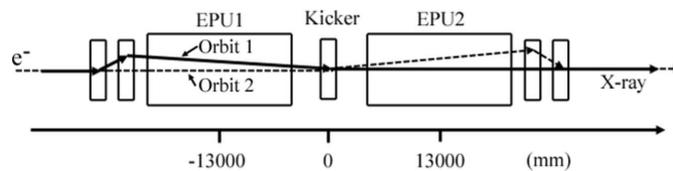

Figure 1
Twin EPUs switching model.

and the other without. In the first case, such as at the BL25SU beamline at SPring-8 and the 16A beamline at Photon Factory, the entrance slit acts as a second source and eliminates the different influence of the two EPUs on the energy resolution. However, the introduction of such an entrance slit will cause more loss of flux and more space will be needed; therefore, we tend to adopt the second way, as is being used for the I10 beamline at Diamond and the SIM beamline at SLS.

In this paper, we propose a beamline design without an entrance slit and discuss how to easily eliminate the difference in energy resolution, flux and the spot size for the two EPUs. This beamline design is given for covering an energy range of 250–2000 eV, which is popular for magnetic research in the soft X-ray range. It has been proposed for ultra-high-energy resolution (Reininger, 2011; Xue *et al.*, 2014). The key point of this design is that a variable line space (VLS) grating is the only vertical focusing optics, which makes it easy to refocus the beam if the incoming beam is unfocused. Hence, it is a good choice for the design of a beamline with fast polarization switching.

The optical layout of the beamline is shown in Fig. 2. The first optical element, M1, is a meridian cylindrical mirror that takes most of the heat, restrains the high-order harmonic radiations and focuses horizontally the beam onto the exit slit. The plane-grating monochromator situated downstream consists of a plane mirror and selectable VLS plane gratings, which disperses the beam in photon energy and focuses the beam vertically onto the exit slit. Downstream from the exit slit is a pair of Kirkpatrick–Baez (KB) mirrors (Kirkpatrick & Baez, 1948), which refocuses the monochromatic beam onto the sample.

3. Energy resolution correction

The switching frequency of left and right circularly polarized X-rays is often required to be 10 Hz. The different position of each EPU under optimized conditions requires different
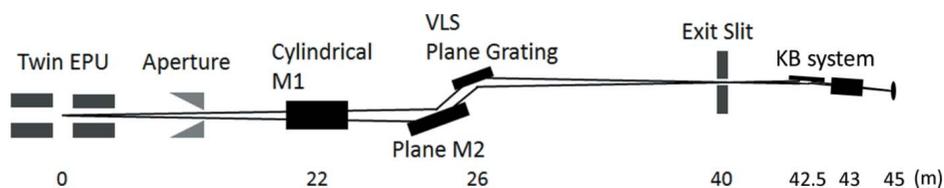

Figure 2
Beamline layout. The distances are measured from the center of the insertion device.

optical setup in the beamline. For a monochromator, this means a fast switching of its incident angle and diffraction angle, which is impractical. To solve this problem, a solution is proposed in this study to find intermediate values for these angles, in which the beamline is not optimized for either of the EPUs. Both of their energy resolutions will be less than their optimal values, but the energy resolution of the two EPUs could be equal.

The line density of a VLS grating is given by

$$k(w) = k_0\left(1 + 2b_2 w + 3b_3 w + \ldots\right), \quad (1)$$

where k_0 is the line density at the grating center and w is the coordinate along the grating length.

The defocus term of the beamline in the optical path function is given by

$$F_{20} = \frac{\cos^2\alpha}{r_1} + \frac{\cos^2\beta}{r_2} - 2b_2 n k_0 \lambda, \quad (2)$$

where λ is the wavelength, α is the incident angle, β is the diffraction angle, n is the diffraction order, r_1 is the distance from the source to the grating and r_2 is the distance from the grating to the exit slit.

As Fig. 1 shows, the distances between the two EPUs to the center of the straight section are +1.3 m and −1.3 m, which means that r_1 is 27300 mm for EPU ID1 and 24700 mm for EPU ID2. The beamline optimized for one EPU by tuning the defocus term to be zero with corresponding r_1 means that for the other EPU it must be far from optimal conditions. This is demonstrated by ray-tracing results at the exit slit obtained with the *SHADOW* software (Welnak *et al.*, 1994), as presented in Fig. 3.

In ray tracing, the angles of the plane mirror and the grating in the monochromator are set according to a virtual light source positioned between the two EPUs. The grating has a central line density of 800 lines mm^{-1}, operated with a c_{ff} value of 2.3 and an exit slit width of 15 µm.

Generally, the energy resolution in this design is determined by five factors: source size, exit slit size, meridian slope error of the grating, meridian slope error of the plane mirror and aberration. The contribution of these factors to the total energy resolution, ΔE_{total}, are given by

$$\Delta E_{total} = \left(\Delta E_{so}^2 + \Delta E_{ex}^2 + \Delta E_{gr}^2 + \Delta E_{pm}^2 + \Delta E_{ab}^2\right)^{1/2}, \quad (3)$$

where

$$\Delta E_{so} = \frac{2.7\Sigma_y \cos(\alpha)E}{nkr_1\lambda}, \quad (4)$$

$$\Delta E_{ex} = \frac{s\cos(\beta)E}{nkr_2\lambda}, \quad (5)$$

$$\Delta E_{gr} = \frac{5.4\sigma_{gr}E}{nk\lambda}\cos\left(\frac{\alpha+\beta}{2}\right)\cos\left(\frac{\alpha-\beta}{2}\right), \quad (6)$$
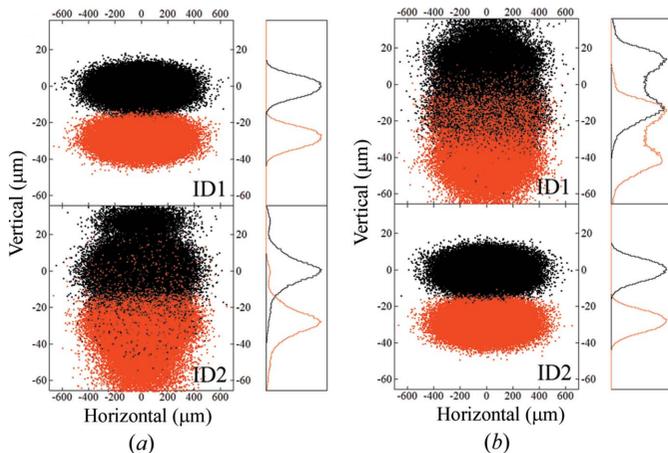
$$\Delta E_{pm} \approx \frac{5.4\sigma_{pm}\cos(\alpha)E}{nk\lambda}, \quad (7)$$

and Σy is the RMS value of the source size, E is the photon energy, σ_{gr} and σ_{pm} are the meridian RMS slope errors of the grating and plane mirror, respectively, and s is the exit slit size. $\Delta E_{ab} = E(\Delta\lambda_{ab}/\lambda)$ and the wavelength dispersion caused by various aberrations can be expressed as
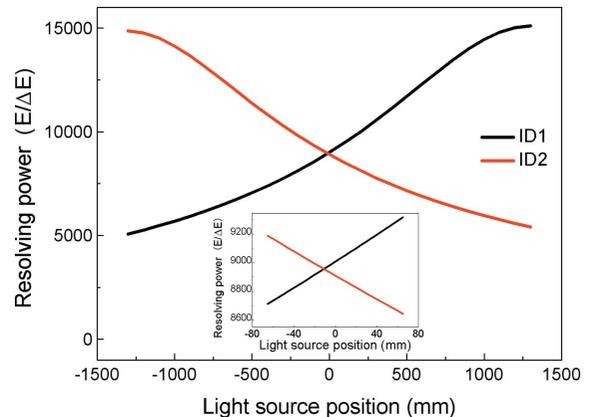
$$\Delta\lambda_{ab} = \frac{d}{m}\left(wF_{20} + \frac{3}{2}w^2 F_{30} + \frac{1}{2}l^2 F_{12} + \frac{1}{2}w^3 F_{40} + \ldots\right). \quad (8)$$

As neither of the two EPUs is under their optimal condition, all of the terms F_{20} (defocus), F_{30} (coma) and F_{40} (spherical aberration) for the two EPUs are not equal to zero. Except F_{12} and F_{40}, the other two terms cannot be ignored. The aberrations strongly affect the energy resolution. The results of the energy resolving power (RP) of the beamline with each individual EPU as a source are presented in Fig. 4.

From Fig. 4, it can be seen that, if setting the midpoint of the straight section as the position of the light source, the RPs of the beam emitted from two EPUs show a slight difference (shown in the inset). This comes only from the contributions of source size and exit slit size [formulae (4) and (5)]. The slope errors accounted for in formulae (6) and (7) are statistical averaged, which is applicable in the focusing case. The
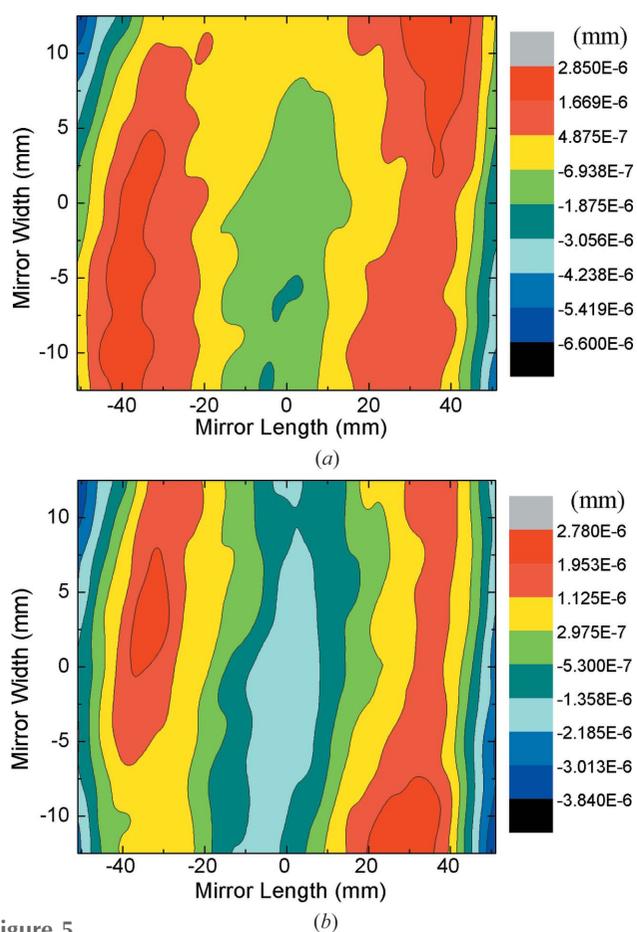

Figure 3
Ray tracings at the exit slit emitted from two EPUs, ID1 and ID2, at 1000.00 eV and 1000.1 eV with different beamline optimization: (*a*) optimized for ID1 and (*b*) optimized for ID2.
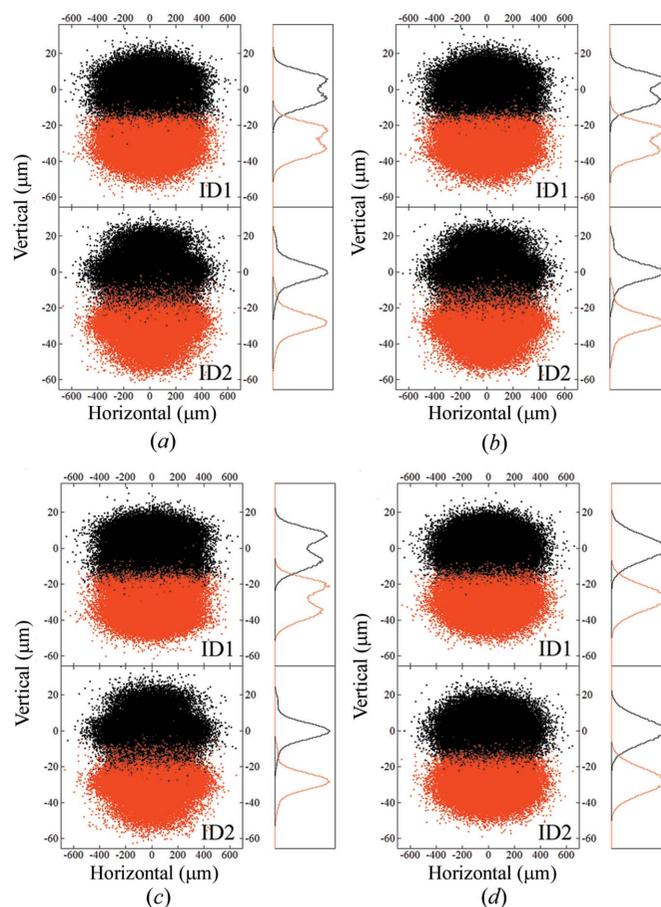

Figure 4
Energy resolving power of the beamline optimized at various positions of a virtual light source for the EPUs ID1 and ID2.

formulae (6) and (7) are not applicable in the unfocused case because the structure of the slope error would be exaggerated over the spot profile if the beam was not focused at the exit slit.

In order to reflect the actual deterioration due to surface error on the unfocused case, ray tracings must be carried out with real surface error data. Fig. 5 shows the contour plots of two sets of real surface error data, marked as #1 and #2, from the measurement of two grating substrates manufactured and tested by Zeiss and installed at the BL09U beamline at Shanghai Synchrotron Radiation Facility (SSRF). The ray-tracing results at the exit slit plane when optimized at the midpoint of the straight section hosting two EPUs are shown in Fig. 6. In Figs. 6(a) and 6(b), the surface error is introduced only on the grating substrate, data #1 and data #2, respectively. In Fig. 6(c), the surface error is introduced both on the plane mirror and the grating substrate. For comparison, a ray tracing under the same condition except without any surface error is shown in Fig. 6(d). As Fig. 6(a) shows, with the surface error on the grating considered, the ray tracing on the energy resolution for EPUs ID1 and ID2 gives dramatically different beam profiles. The energy distribution curve for ID1 has a double-peak structure yet for ID2 only a single peak. With a fixed exit slit of 15 μm, both energy distribution curves (shown at the side of each view) can be fitted with Gaussian profile.

Figure 6
Ray tracings at the exit slit plane at 1000.0 eV and 1000.1 eV: (a) with surface error data #1 on the grating, (b) with surface error data #2 on the grating, (c) with surface error data #2 on the plane mirror and surface error data #1 on the grating and (d) without surface error. The grating has a ruling density of 800 lines mm^{-1} at its center and is operated with c_{ff} 2.3.

The energy resolving powers derived are 12317 for ID1 and 16578 for ID2, respectively. The difference ratio is 35%. With another set of surface error data (#2) for the grating (Fig. 6b) or both for the plane mirror and the grating (Fig. 6c), the difference ratio is as large as in Fig. 6(a). In contrast, without introducing any surface error on the grating and the plane mirror (Fig. 6d), the difference in the resolving power is minimal, coinciding with the calculation in Fig. 4. In addition, ray tracings for another grating with a central line density of 1200 lines mm^{-1} are performed, with the results presented in Fig. 7. The results show the same trends as those in Fig. 6. A large difference in the energy resolution of the two EPUs occurs when surface errors are present on the grating and the plane mirror.

From Figs. 6 and 7 it can be concluded that a real slope error of the grating, and/or the plane mirror, will cause a large difference in the energy resolution for the two EPUs when the virtual light source is set at the midpoint of the two EPUs. As a result, the midpoint is not a good choice to obtain an equal energy resolution for the two EPUs.

It is crucial for the success of the XMCD method to find an optimal position for the virtual light source. Ideally at this position the energy resolution of the two EPUs should be

Figure 5
Contour plots of the surface error data of two real grating substrates, which were fabricated and tested by Zeiss: (a) data #1 and (b) data #2.
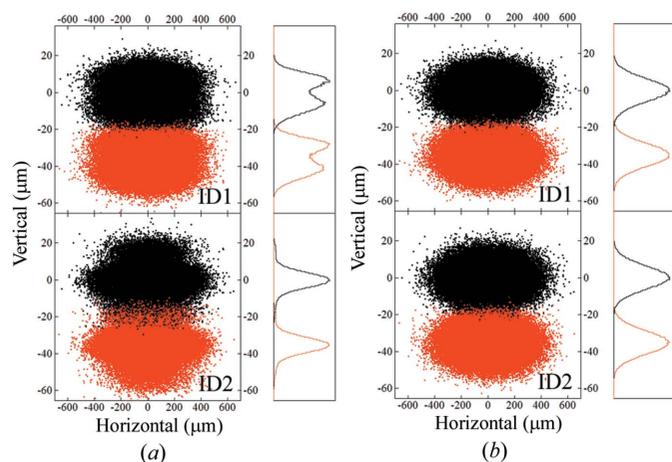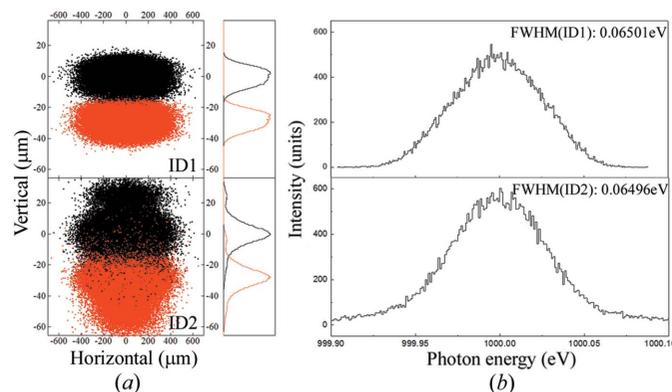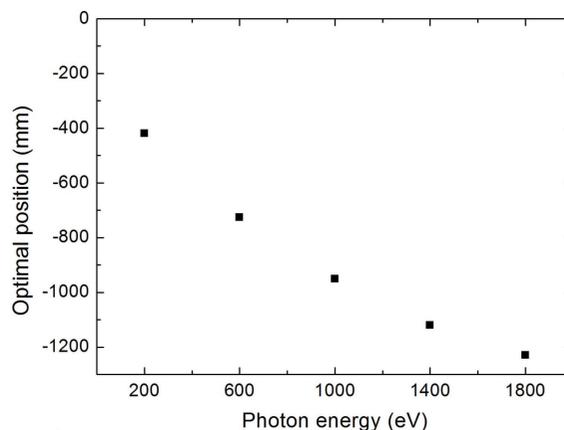
Figure 7
Ray tracings at the exit slit plane at 1000.00 eV and 1000.1 eV. The grating has 1200 lines mm^{-1} at its center and is operated with c_{ff} 2.6: (a) with surface error data #1 on the grating and surface error data #2 on the plane mirror and (b) without surface error.
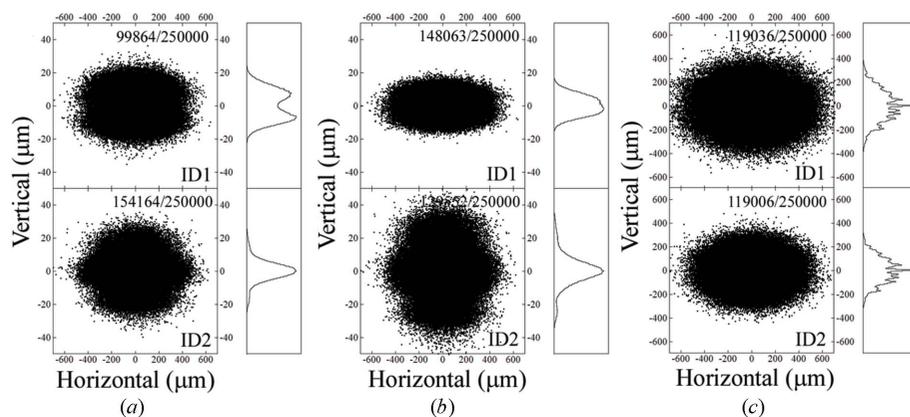

Figure 9
Optimal position of the virtual light source as a function of the photon energy. The position is measured from the center of straight section.

equal, which we call an intermediate state. With the current beamline setup, the position of a virtual light source is defined by the angles of the plane mirror and the grating in the monochromator. By tuning these angles and comparing the consequent energy resolution through the line width of the energy distribution curve obtained from ray tracing, an optimal position of the virtual light source for a photon energy can be located. An example is demonstrated at $h\nu$ = 1000 eV in Fig. 8. It turns out that when the position of the virtual light source is set as −951 mm, the energy resolutions for the two EPUs are equal within error: the full width at half-maximum (FWHM) for EPU ID1 is 0.0643 eV and for EPU ID2 it is 0.0644 eV. This position corresponds to a c_{ff} change from 2.3 to 2.288, and the required angle changes are 0.00768° and 0.00335° for the plane mirror and the grating, respectively. It means that such an adjustment for accomplishing an equal energy resolution can be performed very easily and efficiently. It is noteworthy that, although the beam profiles of the two EPUs look different, the energy resolutions can match well. In

Figure 8
(a) Ray tracing at the exit slit plane at 1000 eV whereby the optimal position is located at −951 mm. (b) Energy distribution curves of the beam spots from two EPUs, all fitted with a Gaussian profile. The full width at half-maximum (FWHM) of the Gaussian profile is shown. The exit slit width is fixed at 15 μm.

the same way, the optimized positions for the virtual light source for a photon energy range from 200 eV to 1800 eV are found and shown in Fig. 9. The position deviates from the midpoint of the two EPUs much further when the energy increases. This is due to the fact that at higher photon energies the grating becomes more grazing incident and there is more contribution of the grating slope error on the energy resolution.
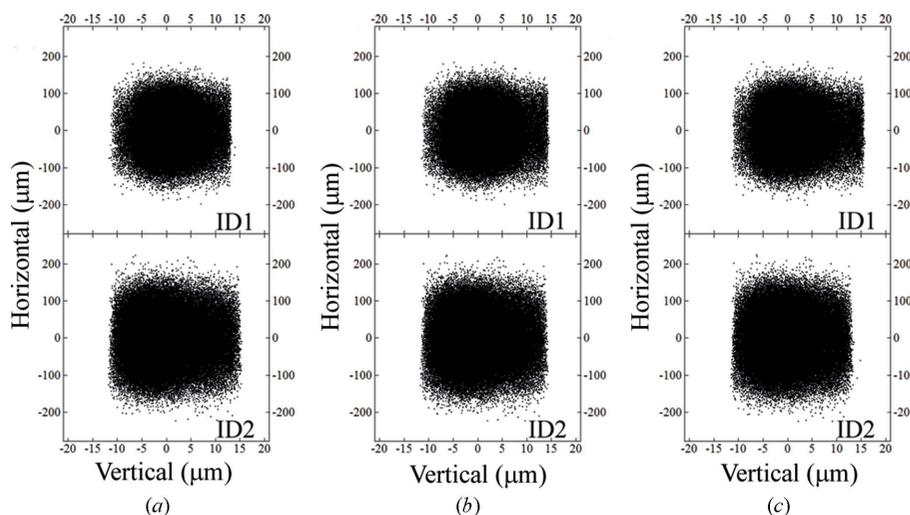
4. Flux and spot size correction

Besides the energy resolution, it is also important to make the individual flux at the sample equal from the two EPUs in order to carry out a satisfactory XMCD measurement. However, on account of their different positions, the flux from each EPU after the exit slit is different. This is shown with photon energy $h\nu$ = 1000 eV as an example through ray tracing in Fig. 10. When setting the virtual light source at the midpoint of the two EPUs (Fig. 10a), the number of rays through the exit slit are 99864 and 154164 for ID1 and ID2, respectively. Such a 54% flux difference will definitely hamper an XMCD experiment. With an intermediate position for the virtual light source (Fig. 10b), the number of rays (148063 and 129552) through the exit slit are getting close, yet still there is 14% difference in flux. To overcome such a flux mismatch, we propose to dislocate the X and the Y blades along the beam: the Y blades remain in the original focal plane, the X blades are relayed downstream, movable by photon energy, to tune the flux from each EPU as equal. The feasibility of such a solution is shown in Fig. 10(c): the Y blades stay in the focal plane, the X blades are relocated 1450 mm downstream with the virtual light source at the intermediate position. The number of rays reaching the sample is 119036 for ID1 and 119006 for ID2. An equal flux between two EPUs is achieved.

To measure the dichroism of an inhomogeneous sample, it is also important to ensure the spot sizes on the sample for the two EPUs are equal. The beamline has been optimized to obtain equal energy resolution and equal flux for the two EPUs after the exit slit as mentioned above. However, the spot sizes at the sample position for the two EPUs are different, as

Figure 10
Ray tracings at the exit slit plane at 1000.0 eV with various position of the virtual light source: (*a*) at the midpoint of two EPUs, (*b*) at the optimized position (−951 mm) and (*c*) at the optimized position (−951 mm) and the *X* blades located at 41.45 m. Surface error data #1 on the grating and surface error data #2 on the plane mirror are introduced.

5. Conclusion

To apply fast polarization switching tandem twin EPUs successfully in XMCD experiments, it is critical to make the energy resolution, the flux and the spot size at the sample from the two EPUs equal. Ray-tracing results show that the energy resolution of the two EPUs shows a large difference when the real surface profiles for optics are included. A conceptually new design to solve this problem is proposed. A VLS plane grating is the only vertical focusing optics before the exit slit, making it possible to adjust the energy resolution of the two EPUs to be equal by tuning the monochromator. After tuning the angles of the plane mirror and the grating to intermediate values, whereby the virtual source does not sit at the midpoint of the two EPUs, the energy resolution of the two EPUs can be equal at every energy. Furthermore, a flux balancing approach is proposed by dislocating the *X* and the *Y* blades in the exit slit and setting the movable *X* blades by energy along the beams. Finally, a spot size balancing approach is also proposed by moving the sample position downstream. With such optimized equal energy resolution, flux and spot size from two EPUs, this beamline design is able to deliver reliable results for XMCD experiments.

shown in Fig. 11(*a*). It can be seen that the spot sizes are almost equal in the horizontal direction with a difference of less than 10%. However, in the vertical direction, the spot size for ID1 is rather smaller than for ID2, which will result in a serious error in the dichroism spectrum. This problem could be relaxed by moving the sample along the beam. As the sample moves downstream, the vertical spot size for ID1 increases and that for ID2 decreases. When the sample moves by 10 mm from its original position, the vertical spot sizes for the two EPUs become equal, as shown in Fig. 11(*b*). By moving another 10 mm more, the vertical spot size for ID1 becomes larger than ID2 (Fig. 11*c*). The horizontal spot sizes for the two EPUs remain almost unchanged during the sample movement. For more challenging samples, with smaller domains of less than 200 µm × 20 µm (spot size), the subtle difference in spot sizes will admittedly make the measurement for dichroism difficult.

Figure 11
Ray tracings on the sample plane at 1000.0 eV with various sample positions: (*a*) sample located at 45 m, (*b*) sample located at 45.01 m and (*c*) sample located at 45.02 m. Surface error data on both KB mirrors are introduced.

References

Agui, A. *et al.*, (2001). *J. Jpn. Soc. Synchrotron Radiat. Res.* **14**, 339.
Chavanne, J., Elleaume, P. & Van Vaerenbergh, P. (1998). *J. Synchrotron Rad.* **5**, 196–201.
Hara, T., Shirasawa, K., Takeuchi, M., Seike, T., Saito, Y., Muro, T. & Kitamura, H. (2003). *Nucl. Instrum. Methods Phys. Res. A*, **498**, 496–502.
Hara, T., Tanaka, T., Tanabe, T., Maréchal, X.-M., Kumagai, K. & Kitamura, H. (1998). *J. Synchrotron Rad.* **5**, 426–427.
Kirkpatrick, P. & Baez, A. V. (1948). *J. Opt. Soc. Am.* **38**, 766–774.
Muro, T., Nakamura, T., Matsushita, T., Kimura, H., Nakatani, T., Hirono, T.,

Kudo, T., Kobayashi, K., Saitoh, Y., Takeuchi, M., Hara, T., Shirasawa, K. & Kitamura, H. (2005). *J. Electron Spectrosc. Relat. Phenom.* **144–147**, 1101–1103.

Reininger, R. (2011). *Nucl. Instrum. Methods Phys. Res. A*, **649**, 139–143.

Saitoh, Y., Kimura, H., Suzuki, Y., Nakatani, T., Matsushita, T., Muro, T., Miyahara, T., Fujisawa, M., Soda, K., Ueda, S., Harada, H., Kotsugi, M., Sekiyama, A. & Suga, S. (2000). *Rev. Sci. Instrum.* **71**, 3254–3259.

Saitoh, Y., Nakatani, T., Matsushita, T., Miyahara, T., Fujisawa, M., Soda, K., Muro, T., Ueda, S., Harada, H., Sekiyama, A., Imada, S., Daimon, H. & Suga, S. (1998). *J. Synchrotron Rad.* **5**, 542–544.

Sawhney, K. J. S., Senf, F., Scheer, M., Schäfers, F., Bahrdt, J., Gaupp, A. & Gudat, W. (1997). *Nucl. Instrum. Methods Phys. Res. A*, **390**, 395–402.

Schmidt, T., Ingold, G., Imhof, A., Patterson, B. D., Patthey, L., Quitmann, C., Schulze-Briese, C. & Abela, R. (2001). *Nucl. Instrum. Methods Phys. Res. A*, **126**, 467–468.

Tanaka, T., Shirasawa, K. & Kitamura, H. (2002). *Rev. Sci. Instrum.* **73**, 1724–1727.

Weiss, M. R., Follath, R., Sawhney, K. J. S., Senf, F., Bahrdt, J., Frentrup, W., Gaupp, A., Sasaki, S., Scheer, M., Mertins, H.-C., Abramsohn, D., Schafers, F., Kuch, W. & Mahler, W. (2001). *Nucl. Instrum. Methods Phys. Res. A*, **449**, 467–468.

Welnak, C., Chen, G. J. & Cerrina, F. (1994). *Nucl. Instrum. Methods Phys. Res. A*, **347**, 344–347.

Xue, L., Reininger, R., Wu, Y.-Q., Zou, Y., Xu, Z.-M., Shi, Y.-B., Dong, J., Ding, H., Sun, J.-L., Guo, F.-Z., Wang, Y. & Tai, R.-Z. (2014). *J. Synchrotron Rad.* **21**, 273–279.